Supplemental material for "β decay of the ground state and of a low-lying isomer in ^{216}Bi"

B. Andel,[1,*] A. N. Andreyev,[2,3] A. Blazhev,[4] R. Lică,[5] H. Naïdja,[6] M. Stryjczyk,[7,8] P. Van Duppen,[7] A. Algora,[9,10] S. Antalic,[1] A. Barzakh,[11] J. Benito,[12] G. Benzoni,[13] T. Berry,[14] M. J. G. Borge,[15] K. Chrysalidis,[16] C. Clisu,[5] C. Costache,[5] J. G. Cubiss,[2] H. De Witte,[7] D. V. Fedorov,[11] V. N. Fedosseev,[16] L. M. Fraile,[12] H. O. U. Fynbo,[17] P. T. Greenlees,[8] L. J. Harkness-Brennan,[18] M. Huyse,[7] A. Illana,[19] J. Jolie,[4] D. S. Judson,[18] J. Konki,[8] I. Lazarus,[20] M. Madurga,[16] N. Marginean,[5] R. Marginean,[5] B. A. Marsh,[16,†] C. Mihai,[5] P. L. Molkanov,[11] P. Mosat,[1] J. R. Murias,[12,21] E. Nacher,[9] A. Negret,[5] R. D. Page,[18] S. Pascu,[5] A. Perea,[15] V. Pucknell,[20] P. Rahkila,[8] E. Rapisarda,[16] K. Rezynkina,[7,22] V. Sánchez-Tembleque,[12] K. Schomacker,[4] M. D. Seliverstov,[11] C. Sotty,[5] L. Stan,[5] C. Sürder,[23] O. Tengblad,[15] V. Vedia,[12] S. Viñals,[15] R. Wadsworth,[2] and N. Warr[4]

(IDS Collaboration)

[1] *Department of Nuclear Physics and Biophysics, Comenius University in Bratislava, 84248 Bratislava, Slovakia*
[2] *School of Physics, Engineering and Technology, York YO10 5DD, United Kingdom*
[3] *Advanced Science Research Center, Japan Atomic Energy Agency, Tokai-mura, Ibaraki 319-1195, Japan*
[4] *Institut für Kernphysik, Universität zu Köln, 50937 Köln, Germany*
[5] *"Horia Hulubei" National Institute for R & D in Physics and Nuclear Engineering, RO-077125 Bucharest, Romania*
[6] *Laboratoire de Physique Mathématique et Physique Subatomique, Université Constantine 1, Constantine 25000, Algeria*
[7] *KU Leuven, Instituut voor Kern- en Stralingsfysica, B-3001 Leuven, Belgium*
[8] *University of Jyvaskyla, Department of Physics, Accelerator laboratory, P.O. Box 35(YFL) FI-40014 University of Jyvaskyla, Finland*
[9] *Instituto de Física Corpuscular, CSIC - Universidad de Valencia, E-46980, Valencia, Spain*
[10] *Institute of Nuclear Research (ATOMKI), P.O.Box 51, H-4001 Debrecen, Hungary*
[11] *Affiliated with an institute covered by a cooperation agreement with CERN*
[12] *Grupo de Física Nuclear, Universidad Complutense de Madrid, 28040, Madrid, Spain*
[13] *Istituto Nazionale di Fisica Nucleare, Sezione di Milano, I-20133 Milano, Italy*
[14] *Department of Physics, University of Surrey, Guildford GU2 7XH, United Kingdom*
[15] *Instituto de Estructura de la Materia, CSIC, Serrano 113 bis, E-28006 Madrid, Spain*
[16] *CERN, CH-1211 Geneve 23, Switzerland*
[17] *Department of Physics and Astronomy, Aarhus University, DK-8000 Aarhus C, Denmark*
[18] *Department of Physics, Oliver Lodge Laboratory, University of Liverpool, Liverpool L69 7ZE, United Kingdom*
[19] *Instituto Nazionale di Fisica Nucleare, Laboratori Nazionali di Legnaro, I-35020 Legnaro, Italy*
[20] *STFC Daresbury, Daresbury, Warrington WA4 4AD, United Kingdom*
[21] *Institut Laue-Langevin, CS 20156, 38042 Grenoble Cedex 9, France*
[22] *Université de Strasbourg, CNRS, IPHC UMR7178, F-67000, Strasbourg, France*
[23] *Institut für Kernphysik, Technische Universität Darmstadt, 64289 Darmstadt, Germany*

* boris.andel@fmph.uniba.sk
† Deceased

TABLE I. Measured γ-ray energies, literature values and corresponding differences for various transitions following decays of natural background and contamination in the beam. All transitions follow β^- decay of listed isotopes, or β^+/EC decay in the case of ^{78}Br, ^{132}Cs, ^{138}La and ^{40}K.

E_γ (keV)	$E_{\gamma,\mathrm{ref}}$ (keV)	Difference (keV)	Isotope	Ref.
238.582(5)	238.632(2)	-0.050(5)	^{212}Pb	[1]
295.28(3)	295.224(2)	0.06(3)	^{214}Pb	[2]
352.016(16)	351.932(21)	0.08(3)	^{214}Pb	[2]
609.408(8)	609.321(7)	0.087(11)	^{214}Bi	[2]
613.725(4)	613.68(7)	0.05(7)	^{78}Br	[3]
667.812(3)	667.714(2)	0.098(4)	^{132}Cs	[4]
795.727(4)	795.864(4)	-0.137(6)	^{134}Cs	[5]
881.574(16)	881.6(1)	-0.03(10)	^{84}Br	[6]
1120.340(16)	1120.294(6)	0.046(17)	^{214}Bi	[2]
1435.850(8)	1435.77(7)	0.08(7)	^{138}La	[7]
1460.900(5)	1460.851(6)	0.049(8)	^{40}K	[8]
1729.65(5)	1729.595(15)	0.06(5)	^{214}Bi	[2]
1764.590(12)	1764.491(14)	0.099(18)	^{214}Bi	[2]
1847.61(5)	1847.433(17)	0.18(5)	^{214}Bi	[2]
2118.65(8)	2118.513(25)	0.14(8)	^{214}Bi	[2]
2204.20(2)	2204.10(4)	0.10(5)	^{214}Bi	[2]
2447.79(6)	2447.69(3)	0.10(7)	^{214}Bi	[2]
2614.810(8)	2614.511(10)	0.299(13)	^{208}Tl	[9]
2751.44(7)	2751.06(15)	0.38(16)	^{86}Br	[10]
2926.05(35)	2925.93(20)	0.12(41)	^{86}Br	[10]

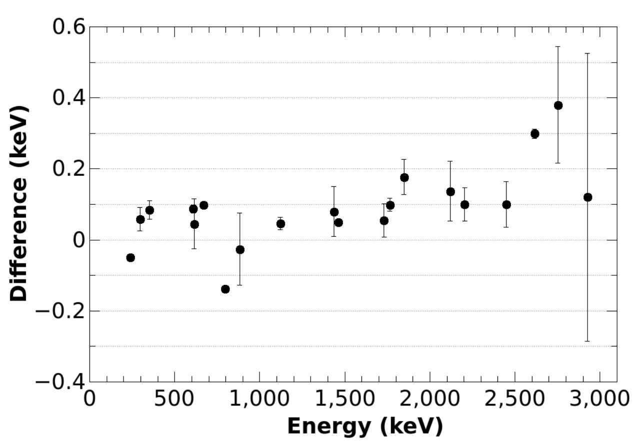

FIG. 1. Measured γ-ray energies and corresponding differences with the literature values for transitions from Table I.

TABLE II. List of summing peaks marked in γ-ray spectra in the manuscript, and γ or x rays forming these peaks.

E_{sum} (keV)	E of summed γ or x rays (keV)
438	360+≈79(Po x rays)
475	223+251
498	419+≈79(Po x rays)
583	223+360
611	251+360
642	223+419
670	251+419
698	148+550
773	223+550
778	360+419
909	360+550
969	419+550
1101	419+683
1232	550+683

TABLE III. γ-ray transitions following the β^- decay of ^{216}Bi^g. E_i, E_f, and E_γ are the respective energies of the initial and the final level and of the γ-ray transition connecting the levels. I_γ and I_t are the γ-ray and transition intensities, relative to the intensity of the 359.6-keV γ ray and transition, respectively. Internal conversion coefficients ($\alpha_{\rm tot}$) used to deduce I_t were calculated from $\alpha_{\rm tot,th}$ from Ref. [11], except for the experimental value for the 486.1-keV transition. The last column notes different approaches to obtain or estimate $\alpha_{\rm tot}$, see the main text for details. Tentative levels or transitions are written in italic. Double dagger (‡) marks values, which were deduced from γ-γ coincidences.

E_i (keV)	E_f (keV)	E_γ (keV)	I_γ	I_t	$\alpha_{\rm tot}$ [11]	Note
549.8(2)	0	549.8(2)	-	-	0.0257(4)	$E2$
968.6(3)	549.8(2)	418.8(2)	-	-	0.0498(7)	$E2$
1328.2(3)	968.6(3)	359.6(2)	100	100	0.0748(11)	$E2$
1551.5(4)	1328.2(3)	223.3(2)	74.4(5)	91.5(7)	0.322(5)	$E2$
1611.5(3)	1328.2(3)	283.3(3)‡	0.7(2)‡	0.8(3)‡	0.31(28)	$E1$-$M1$
	968.6(3)	642.9(2)‡	1.0(2)‡	1.1(2)‡	0.09(8)	$E1$-$M2$
1699.3(4)	1551.5(4)	147.8(2)	4.05(6)	11(7)	1.9(17)	$E1$-$M1$
1785.7(4)	1328.2(3)	457.5(2)	0.87(4)	0.88(7)	0.09(7)	$E1$-$M1$
1802.7(4)	1551.5(4)	251.2(2)	19.07(12)	25(7)	0.44(39)	$E1$-$M1$
1814.3(4)	1328.2(3)	486.1(3)‡	2.2(7)	4.4(16)	1.1(4)	exp
1873.9(4)	1551.5(4)	322.4(2)	4.82(6)	5.5(9)	0.22(19)	$E1$-$M1$
1890.2(4)	1328.2(3)	562.1(2)‡	1.5(3)‡	1.5(3)‡	0.05(4)	$E1$-$M1$
1979.9(4)	1551.5(4)	428.4(2)	1.91(7)	1.96(17)	0.10(9)	$E1$-$M2$
	1328.2(3)	*651.6(4)*‡	*0.21(11)*‡	*0.21(11)*‡	0.09(8)	$E1$-$M2$
2038.8(4)	1551.5(4)	487.3(2)‡	4.6(7)‡	4.6(8)‡	0.07(6)	$E1$-$M1$
2182.1(5)	1551.5(4)	630.6(2)‡	2.5(4)‡	2.5(5)‡	0.10(9)	$E1$-$M2$
2234.2(4)	1551.5(4)	682.8(2)	11.62(11)	11.6(8)	0.08(7)	$E1$-$M2$
2271.1(3)	*1611.5(3)*	659.6(2)‡	0.69(10)‡	0.69(11)‡	0.084(78)	$E1$-$M2$
	1551.5(4)	719.8(4)‡	0.34(12)‡	0.33(12)‡	0.07(6)	$E1$-$M2$
2338.2(4)	1814.3(4)	523.9(2)	0.49(4)	0.48(4)	0.06(5)	$E1$-$M1$
	1802.7(4)	535.5(3)‡	0.54(15)‡	0.53(15)‡	0.06(5)	$E1$-$M1$
2508.9(5)	1814.3(4)	694.7(2)‡	0.60(3)	0.60(5)	0.072(67)	$E1$-$M2$
2613.6(5)	1551.5(4)	1062.1(3)‡	0.36(12)‡	0.35(11)‡	0.023(20)	$E1$-$M2$
2727.5(4)	1551.5(4)	*1176.0(3)*‡	*0.47(12)*‡	*0.44(11)*‡	*0.017(15)*	$E1$-$M2$
2761.3(5)	1551.5(4)	1209.8(4)‡	0.35(11)‡	0.33(11)‡	0.016(14)	$E1$-$M2$
2850.3(5)	1551.5(4)	1298.9(3)	0.29(4)	0.27(4)	0.013(12)	$E1$-$M2$
-	-	360.4(3)‡	0.7(3)‡	0.7(3)‡	0.16(14)	$E1$-$M1$

TABLE IV: γ-ray transitions following the β^- decay of ^{216}Bi^m. For detailed explanation of the table, see caption of Table III. Intensities I_γ and I_t are relative to the intensity of the 549.8-keV γ ray and transition, respectively. The γ-ray and transition intensities of the 549.8- and 418.8-keV decays were corrected for the indirect feeding from the β^- decay of ^{216}Bi^g. For levels marked by an asterisk it cannot be ruled out that they in fact belong to the β^- decay of ^{216}Bi^g, see the main manuscript for details.

E_i (keV)	E_f (keV)	E_γ (keV)	I_γ	I_t	$\alpha_{\rm tot}$ [11]	Note
549.8(2)	0	549.8(2)	100	100	0.0257(4)	$E2$
968.6(3)	549.8(2)	418.8(2)	43.7(7)	44.7(8)	0.0498(7)	$E2$
1130.6(3)	549.8(2)	580.9(2)‡	12.2(19)‡	12.6(20)‡	0.05(4)	$E1$-$M1$
1328.2(3)	968.6(3)	359.6(2)	-	0.33(13)‡[a]	0.0748(11)	$E2$
1363.8(2)	549.8(2)	814.1(2)‡	3.06(5)	3.12(14)	0.05(4)	$E1$-$M2$
	0	1363.8(3)‡	2.08(6)	2.05(6)	0.012(10)	$E1$-$M2$
1404.5(3)	549.8(2)	854.7(2)	3.87(7)	3.93(16)	0.040(37)	$E1$-$M2$
1503.3(2)	1130.6(3)	372.6(2)‡	0.82(12)‡	0.91(17)‡	0.15(13)	$E1$-$M1$
	968.6(3)	534.9(3)‡	1.33(13)	1.37(15)	0.06(5)	$E1$-$M1$
	549.8(2)	953.5(2)	7.78(9)	7.81(22)	0.030(27)	$E1$-$M2$
	0	*1503.4(2)*	*0.20(3)*	*0.19(3)*	0.009(8)	$E1$-$M2$
1525.4(4)	968.6(3)	556.8(2)‡	1.44(25)‡	1.5(3)‡	0.05(4)	$E1$-$M1$
1627.1(4)	968.6(3)	658.5(2)‡	2.3(4)‡	2.4(4)‡	0.083(78)	$E1$-$M2$
1676.0(3)	549.8(2)	1126.2(2)‡	1.7(3)‡	1.7(3)‡	0.019(17)	$E1$-$M2$
	0	*1676.1(2)*	*0.52(3)*	*0.51(3)*	0.007(6)	$E1$-$M2$
1709.7(1)	1503.3(2)	206.4(3)‡	0.96(23)‡	1.6(7)‡	0.75(67)	$E1$-$M1$
	1404.5(3)	*305.2(2)*‡	*0.38(7)*‡	*0.47(12)*‡	0.26(23)	$E1$-$M1$
	1363.8(2)	345.7(2)‡	0.76(11)‡	0.88(17)‡	0.18(16)	$E1$-$M1$
	1130.6(3)	579.1(2)‡	1.6(3)‡	1.7(3)‡	0.047(39)	$E1$-$M1$
	968.6(3)	741.1(2)	3.32(5)	3.43(19)	0.060(55)	$E1$-$M2$
	549.8(2)	1160.0(2)	7.05(8)	7.00(14)	0.018(16)	$E1$-$M2$
	0	*1710.0(2)*	*0.13(2)*	*0.13(2)*	0.007(6)	$E1$-$M2$
1727.1(2)	1503.3(2)	223.7(2)‡	0.82(16)‡	1.3(5)‡	0.6(5)	$E1$-$M1$
	1130.6(3)	596.8(2)	1.12(6)	1.14(7)	0.044(36)	$E1$-$M1$
	968.6(3)	758.6(2)	12.23(12)	12.6(6)	0.056(52)	$E1$-$M2$
	549.8(2)	1177.3(2)‡	0.55(22)‡	0.54(22)‡	0.017(15)	$E1$-$M2$
1792.2(2)	1363.8(2)	*428.4(3)*‡	*0.24(5)*‡	*0.26(6)*‡	0.10(9)	$E1$-$M1$
	968.6(3)	823.6(2)	4.02(6)	4.10(17)	0.045(41)	$E1$-$M2$
	549.8(2)	1242.5(2)‡	1.7(3)‡	1.7(3)‡	0.015(13)	$E1$-$M2$
1797.5(4)	549.8(2)	1247.7(3)‡	0.72(14)‡	0.72(14)‡	0.015(13)	$E1$-$M2$
1818.0(3)*	1130.6(3)	687.5(2)‡	0.78(15)‡	0.82(17)‡	0.074(69)	$E1$-$M2$
	968.6(3)	849.3(2)‡	1.04(18)‡	1.06(19)‡	0.041(37)	$E1$-$M2$
1875.8(2)	1130.6(3)	745.0(2)	0.80(3)	0.82(5)	0.06(5)	$E1$-$M2$
	549.8(2)	1326.1(2)‡	1.44(25)‡	1.42(25)‡	0.013(11)	$E1$-$M2$
	0	*1875.9(2)*	*0.36(3)*	*0.35(3)*	0.006(4)	$E1$-$M2$
1908.2(2)	1363.8(2)	544.4(3)‡	0.24(5)‡	0.25(5)‡	0.055(47)	$E1$-$M1$
	1328.2(3)	*580.2(3)*‡	*0.32(12)*‡	*0.33(13)*‡	0.05(4)	$E1$-$M1$
	968.6(3)	939.6(2)	1.31(4)	1.31(5)	0.031(28)	$E1$-$M2$
	549.8(2)	1358.5(2)‡	1.7(3)‡	1.7(3)‡	0.012(10)	$E1$-$M2$
1911.8(4)*	968.6(3)	943.2(2)	1.00(8)	1.00(8)	0.031(28)	$E1$-$M2$
1916.7(3)	549.8(2)	1367.0(2)‡	1.23(21)‡	1.21(21)‡	0.012(10)	$E1$-$M2$
1964.3(2)	968.6(3)	995.7(2)	0.71(5)	0.71(6)	0.03(2)	$E1$-$M2$
	549.8(2)	1414.6(2)	0.70(4)	0.69(4)	0.011(9)	$E1$-$M2$
1970.6(4)*	968.6(3)	1002.0(2)‡	1.03(19)‡	1.03(19)‡	0.03(2)	$E1$-$M2$
2010.0(4)	549.8(2)	1460.3(3)‡	0.57(13)‡	0.57(13)‡	0.010(8)	$E1$-$M2$

[a] Corresponds to indirect feeding of the 1328.2-keV level by the 580.2-keV transition.

Continued TABLE IV

E_i (keV)	E_f (keV)	E_γ (keV)	I_γ	I_t	$\alpha_{\rm tot}$ [11]	Note
2031.0(4)	968.6(3)	1062.4(2)‡	2.9(6)‡	2.9(6)‡	0.023(20)	$E1$-$M2$
	549.8(2)	*1481.8(5)*	*0.13(7)*	*0.13(6)*	0.010(8)	$E1$-$M2$
2075.2(4)*	968.6(3)	1106.6(2)	0.78(4)	0.78(4)	0.020(18)	$E1$-$M2$
2083.3(6)	549.8(2)	*1533.6(6)*‡	*0.27(9)*‡	*0.26(9)*‡	0.009(7)	$E1$-$M2$
2114.4(4)	549.8(2)	1564.7(3)‡	0.88(17)‡	0.86(16)‡	0.009(7)	$E1$-$M2$
2179.6(3)	1363.8(2)	815.6(6)‡	0.68(3)	0.69(4)	0.046(42)	$E1$-$M2$
	968.6(3)	1211.0(3)‡	0.53(19)‡	0.53(19)‡	0.016(14)	$E1$-$M2$
	549.8(2)	1630.0(5)‡	0.51(13)‡	0.50(13)‡	0.008(6)	$E1$-$M2$
2282.5(4)*	968.6(3)	1313.9(3)‡	0.56(11)‡	0.55(11)‡	0.013(11)	$E1$-$M2$
*2406.5(4)**	1130.6(3)	*1275.9(3)*	*0.52(12)*‡	*0.51(12)*‡	0.014(12)	$E1$-$M2$
2446.1(3)*	1818.0(3)	628.1(2)‡	0.43(7)‡	0.46(8)‡	0.10(9)	$E1$-$M2$
	1130.6(3)	1315.6(2)‡	0.22(5)‡	0.22(5)‡	0.013(11)	$E1$-$M2$
2476.3(5)	1792.2(2)	684.0(4)‡	0.32(8)‡	0.34(9)‡	0.075(70)	$E1$-$M2$
	549.8(2)	*1926.4(3)*‡	*0.20(6)*‡	*0.20(6)*‡	0.005(4)	$E1$-$M2$
2479.1(3)*	1818.0(3)	660.9(3)‡	0.23(4)‡	0.24(5)‡	0.083(77)	$E1$-$M2$
	1130.6(3)	1348.9(4)‡	0.30(10)‡	0.29(10)‡	0.012(11)	$E1$-$M2$
2570.6(3)	968.6(3)	1602.1(2)‡	0.69(13)‡	0.68(13)‡	0.008(7)	$E1$-$M2$
	549.8(2)	2020.7(3)‡	0.49(10)‡	0.48(10)‡	0.005(4)	$E1$-$M2$
2609.6(4)	549.8(2)	2059.9(3)‡	0.33(8)‡	0.32(7)‡	0.005(3)	$E1$-$M2$
2683.9(2)	968.6(3)	1715.1(2)	0.47(3)	0.46(3)	0.007(5)	$E1$-$M2$
	549.8(2)	2134.3(2)	0.22(3)	0.22(3)	0.004(3)	$E1$-$M2$
2820.7(3)	1130.6(3)	1690.0(3)‡	0.34(7)‡	0.33(7)‡	0.007(6)	$E1$-$M2$
	549.8(2)	2270.9(3)‡	0.77(14)‡	0.76(14)‡	0.004(3)	$E1$-$M2$
2864.1(3)	2010.0(4)	854.5(4)‡	0.15(4)‡	0.15(4)‡	0.040(37)	$E1$-$M2$
	549.8(2)	2314.6(2)	0.30(2)	0.29(2)	0.004(2)	$E1$-$M2$
3096.1(9)	549.8(2)	*2546.4(9)*‡	*0.12(5)*‡	*0.12(5)*‡	0.0032(18)	$E1$-$M2$
3136.0(4)	549.8(2)	*2586.2(3)*	*0.131(13)*	*0.128(13)*	0.0032(17)	$E1$-$M2$
3166.4(9)	549.8(2)	*2616.6(8)*‡	*0.28(13)*‡	*0.27(12)*‡	0.0031(17)	$E1$-$M2$
3290.3(6)	549.8(2)	2740.5(5)‡	0.17(5)‡	0.17(5)‡	0.0029(15)	$E1$-$M2$
3333.9(3)	968.6(3)	2365.1(3)	0.122(16)	0.120(16)	0.004(2)	$E1$-$M2$
	549.8(2)	2784.5(5)‡	0.17(5)‡	0.17(5)‡	0.0029(14)	$E1$-$M2$
3395.9(4)	549.8(2)	2846.1(4)‡	0.10(4)‡	0.10(4)‡	0.0028(13)	$E1$-$M2$

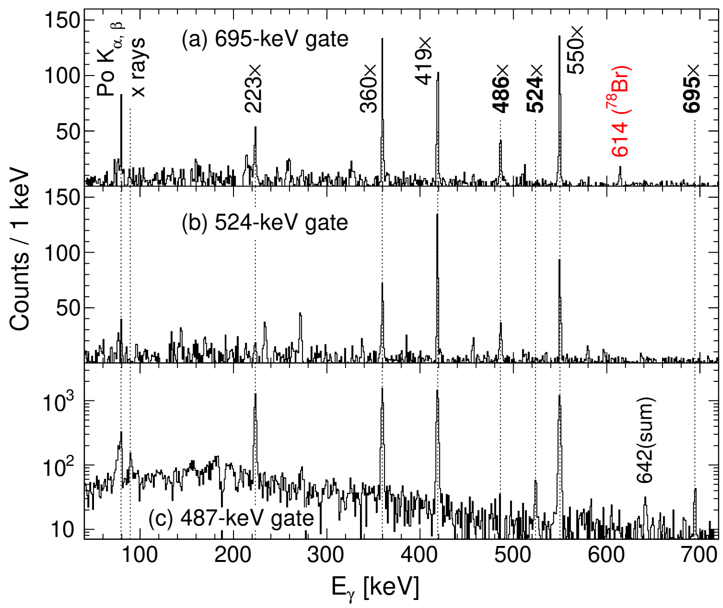

FIG. 2. Background-subtracted γ rays in coincidence with: (a) the 694.7-keV transition, (b) the 523.9-keV transition and (c) the doublet of the 486.1- and 487.3-keV γ rays. Transitions following the β^- decay of ^{216}Bi^g are marked with (×) sign, new transitions are written in bold. The 223-keV peak in panel (a) does not come from the real 694.7-223.3-keV coincidence, but from the partial overlap of the 694.7-keV gate with two weak peaks visible in the 223-keV gate in Fig. 3(a) in the main manuscript. One of the peaks is the 698-keV summing peak (Table II), the other is a weak unassigned 693.7(6)-keV peak. The latter is too weak to originate from coincidence of the 694.7- and 223.3-keV γ rays, as can be seen by comparing with the 694.7-keV peak in Fig. 3(b) in the main manuscript gated on the 359.6-keV transition. The 614-keV peak in panel (a) originates from the 695-614-keV cascade in ^{78}Br [3], which was a contaminant in the beam.

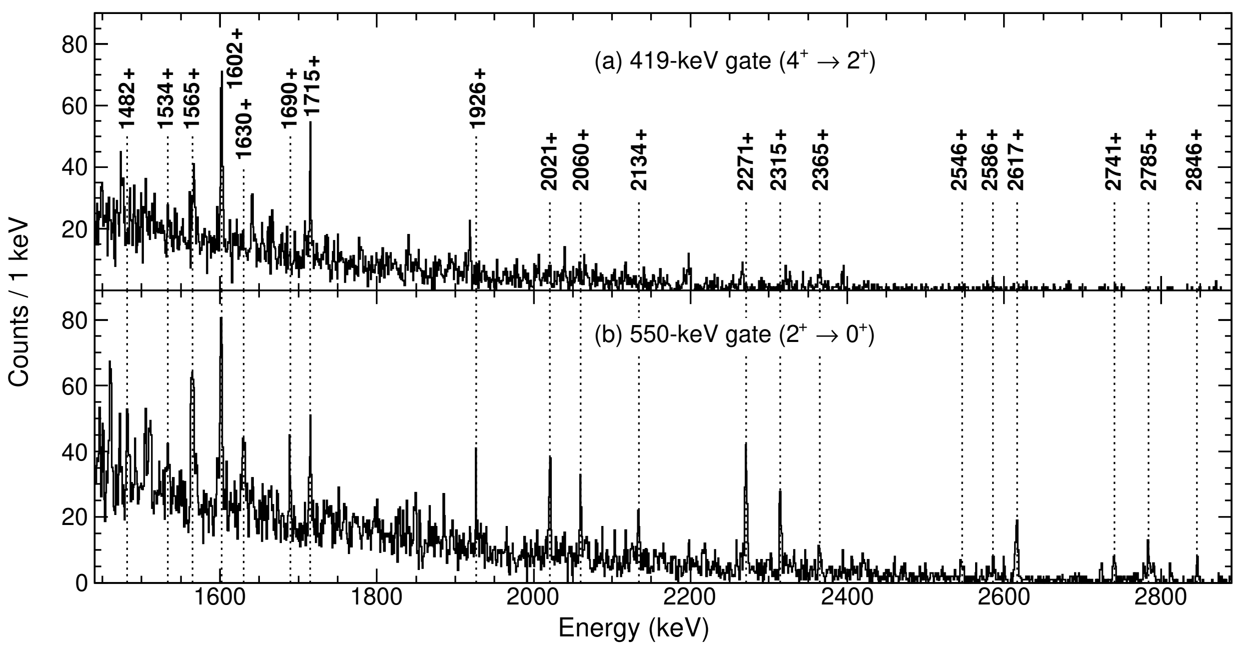

FIG. 3. The 1480–2850-keV energy range of background-subtracted spectra of γ rays in coincidence with: (a) the 418.8-keV $(4^+) \rightarrow 2^+$ and (b) the 549.8-keV $2^+ \rightarrow 0^+$ transition. All labeled peaks are new transitions following β^- decay of ^{216}Bi^m.

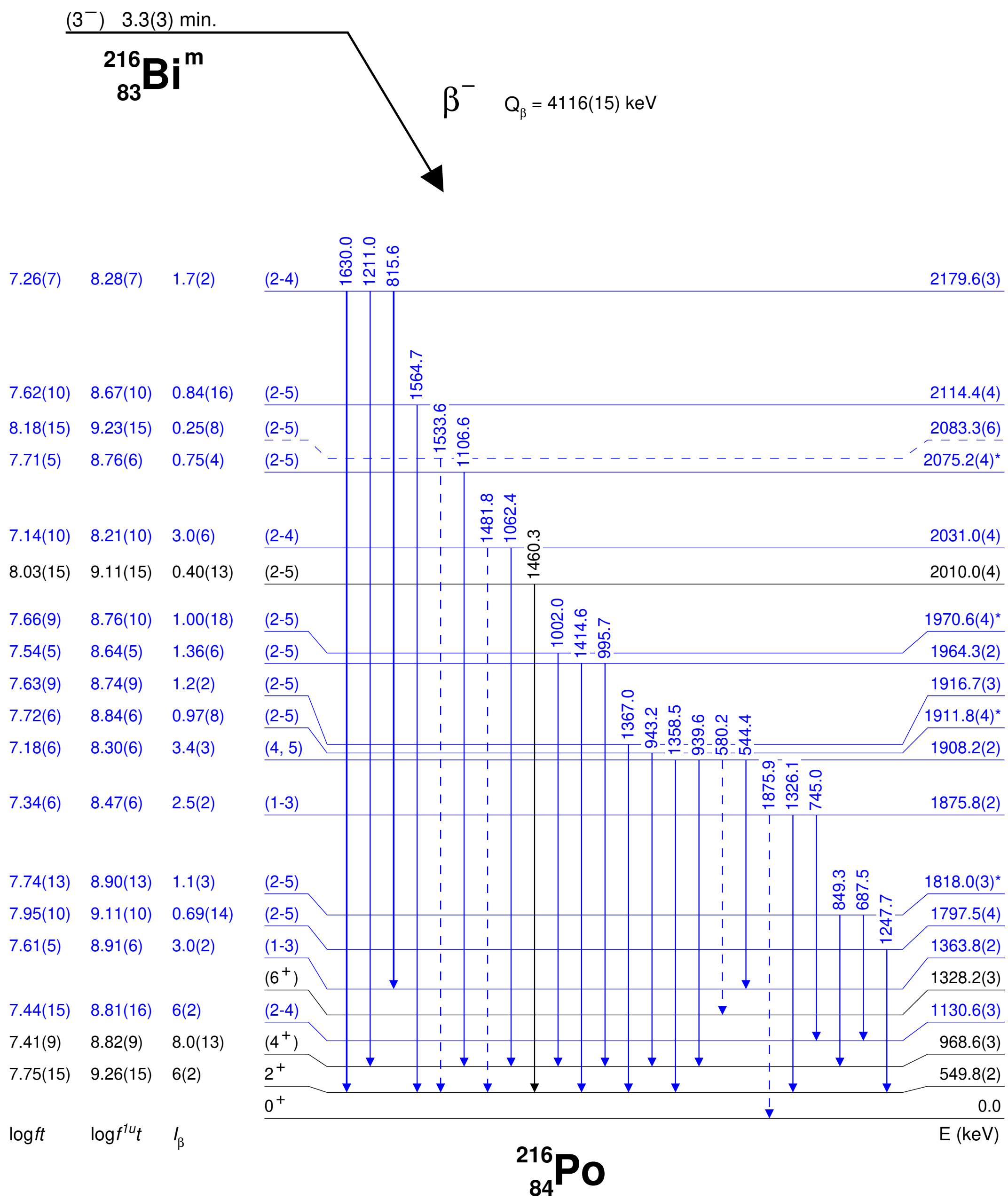

FIG. 4. The second part of the decay scheme with levels in ^{216}Po populated by the β^- decay of ^{216}Bi^m. The new transitions and levels from the present study are highlighted in blue, while those in black font were reported in Ref. [12]. The half-life of ^{216}Bi^m, β-decay feeding intensities and log(ft), log($f^{1u}t$) values are from this work. All spin and parity assignments are from this work, with an exception of the yrast levels in ^{216}Po up to the (6^+) state, which were taken from Ref. [13]. The Q_β value was calculated as the difference between the atomic mass excesses of ^{216}Bi^m and ^{216}Po taken from NUBASE [14]. For display purposes, the levels up to the 1818.1-keV state are spaced evenly. Dashed lines denote tentative levels and transitions. For levels marked with an asterisk it cannot be ruled out that they in fact belong to the β^- decay of ^{216}Bi^g, see the main manuscript for details.

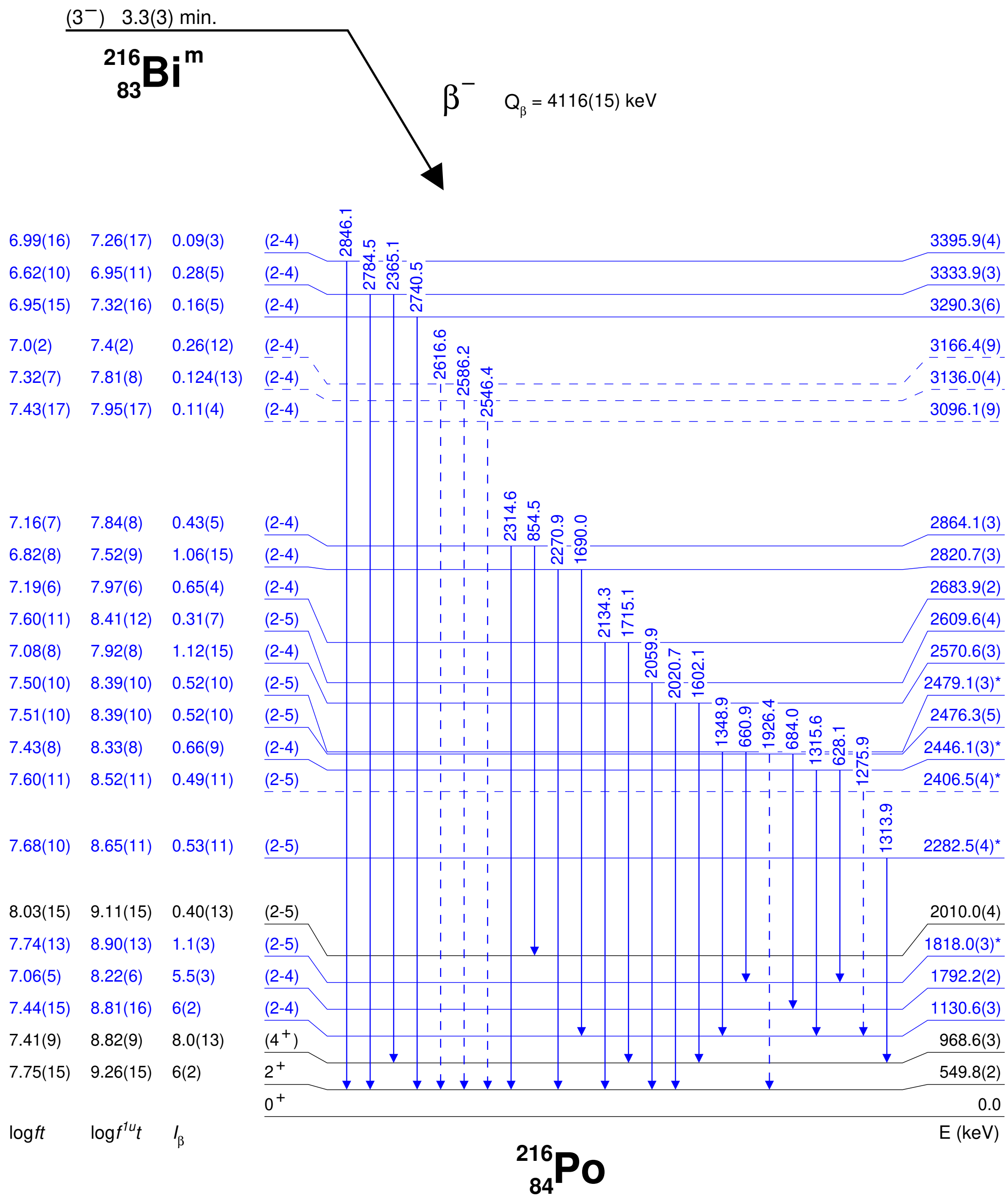

FIG. 5. The third and final part of the decay scheme with levels in ^{216}Po populated by the β^- decay of ^{216}Bi^m. See the caption of Fig. 4 in the main manuscript for detailed description. For display purposes, the levels up to 2010.0-keV state are spaced evenly.

I. SELECTION OF RUNS FOR HALF-LIFE DETERMINATION

Half-lives for ^{78}Br, ^{216}Bi^g and ^{216}Bi^m deduced from the respective measurement runs are listed in Table V. The time distributions for ^{216}Bi^g and ^{216}Bi^m in these runs are shown in Figs. 6, 7, 8, 9 and 10, while the time distributions for ^{78}Br are in Figs. 11, 12, 13, 14 and 15. To have the same conditions for all the cases, each time distribution was fitted by a function $R(1-e^{-\lambda t})+A_0e^{-\lambda t}$, where R, A_0 and λ were free parameters. The term with the R parameter describes the grow-in and saturation part of the distribution, while the term with A_0 is included for the situation when some activity was implanted on the tape before the start of the data acquisition. The same fitting range of 0–2000 s was used for all cases.

To select the measurement runs used for determination of final half-lives in the main manuscript, a result for ^{78}Br consistent with the literature value of 6.45(4) min. [3] within 1σ uncertainty was required. This condition was fulfilled in runs 129, 130 and 132 (Table V). Additionally, the time distributions for ^{216}Bi^g were inspected more closely, because this case has very high statistics and thus it should display the stability of the measurement conditions. Based on the quality of the fit of the ^{216}Bi^g distribution, the run 129 shown in Fig. 7 was also excluded. The number of residuals which are outside the $\pm2\sigma$ interval in Fig. 7(a) from run 129 is significantly higher than in Figs. 8(a) and 10(a) from runs 130 and 132, respectively. The worse quality of the fit is also visible on the largest reduced χ^2 value for the run 129 in Table V. Lastly, the residuals in the first 800 s in Fig. 7(a), which is a crucial part to describe the grow-in part of the time distribution, seem to have a non-random pattern, where in the beginning they are mostly concentrated above 0 and towards the end of this interval they are mostly below 0.

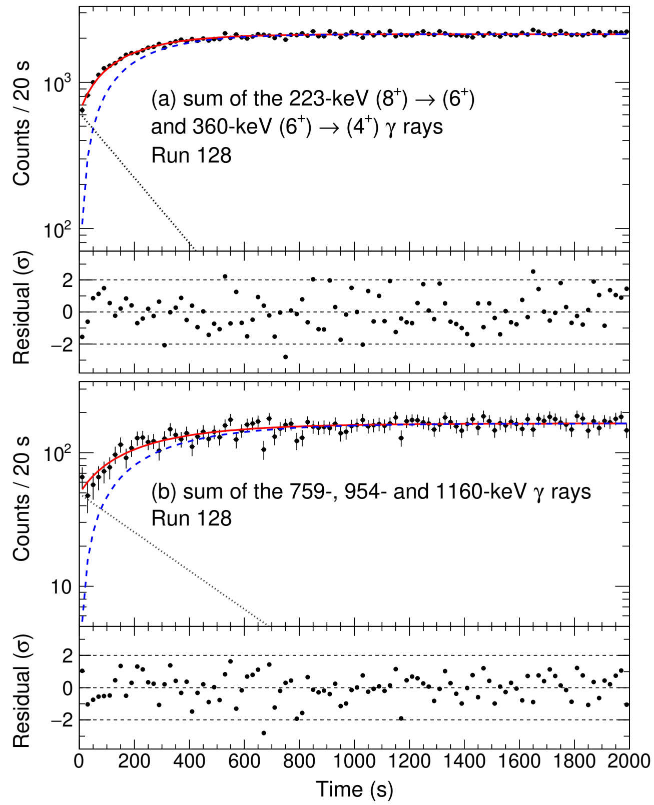

FIG. 6. Background-subtracted time distributions from run 128 for (a) ^{216}Bi^g from sum of the gates on the 223.3- and 359.6-keV γ rays and (b) ^{216}Bi^m from sum of the gates on the 758.6-, 953.5- and 1160.0-keV γ rays. Each distribution was fitted (solid red line) by an exponential growth function (dashed blue line) plus exponential decay function (dotted black line). The corresponding normalized residuals of the fits are plotted below each time distribution, dashed lines in these plots mark values of -2σ, 0σ, and 2σ.

TABLE V. Half-lives for ^{78}Br, ^{216}Bi^{g} and ^{216}Bi^{m} deduced from the respective measurement runs. Reduced χ^2 values from the fits of the time distributions are given next to each column with half-lives.

Run #	$T_{1/2}(^{78}\mathrm{Br})$ (min.)	χ^2/dof	$T_{1/2}(^{216}\mathrm{Bi}^g)$ (min.)	χ^2/dof	$T_{1/2}(^{216}\mathrm{Bi}^m)$ (min.)	χ^2/dof
128	9.7(16)	0.96	2.247(82)	1.20	3.48(50)	0.72
129	6.23(63)	0.97	2.129(70)	1.76	3.26(36)	0.95
130	7.22(79)	0.75	2.147(45)	1.15	3.70(33)	0.96
131	5.36(52)	1.23	1.925(35)	1.25	3.01(29)	1.06
132	6.08(80)	1.01	1.974(37)	1.14	3.07(26)	1.05

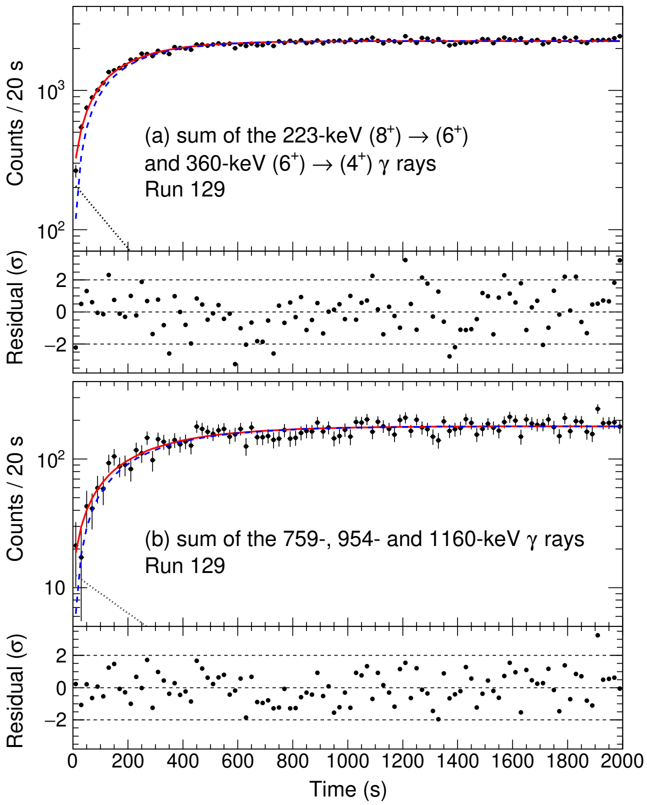

FIG. 7. The same as Fig. 6, but for run 129.

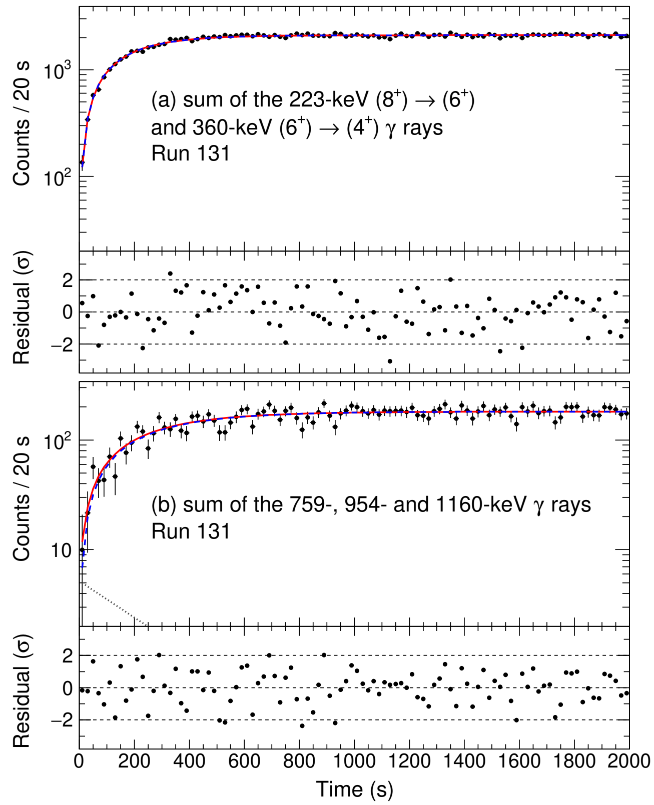

FIG. 9. The same as Fig. 6, but for run 131.

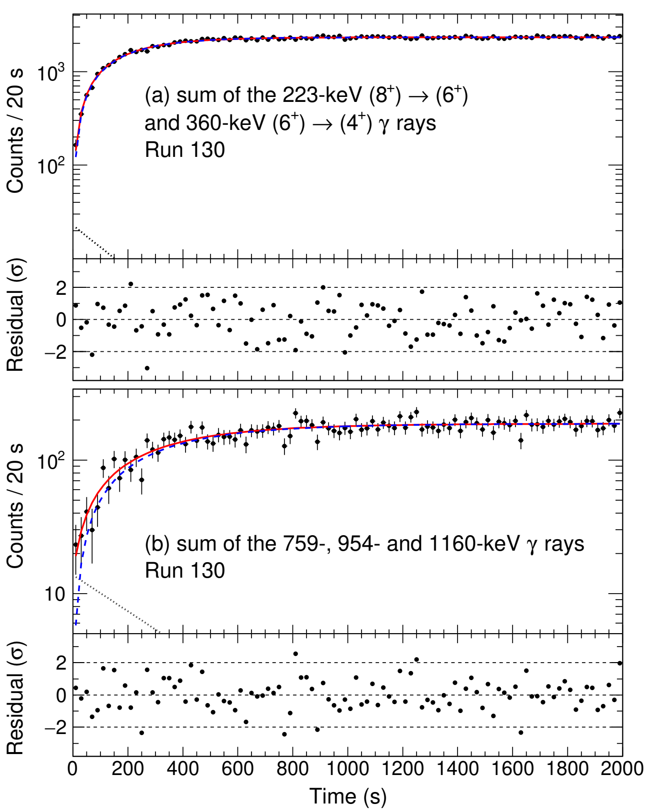

FIG. 8. The same as Fig. 6, but for run 130.

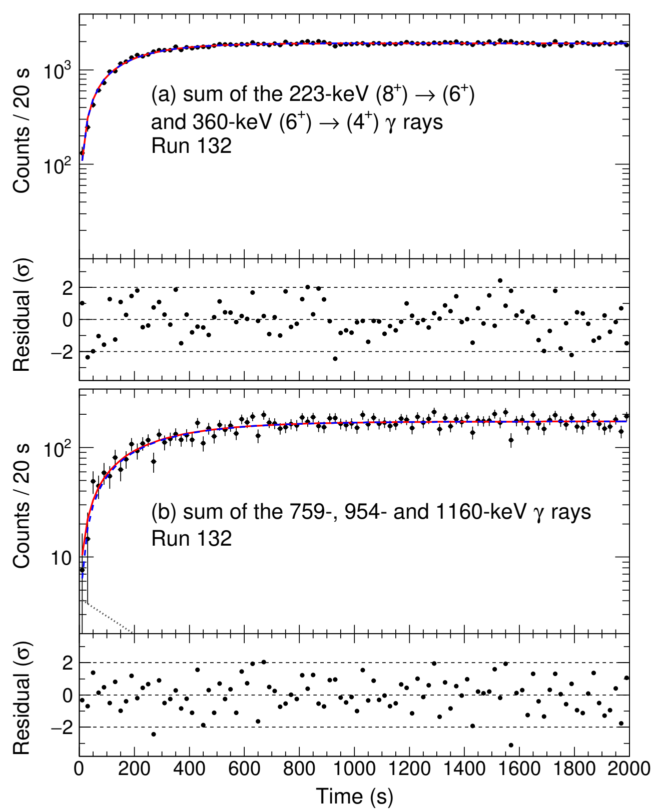

FIG. 10. The same as Fig. 6, but for run 132.

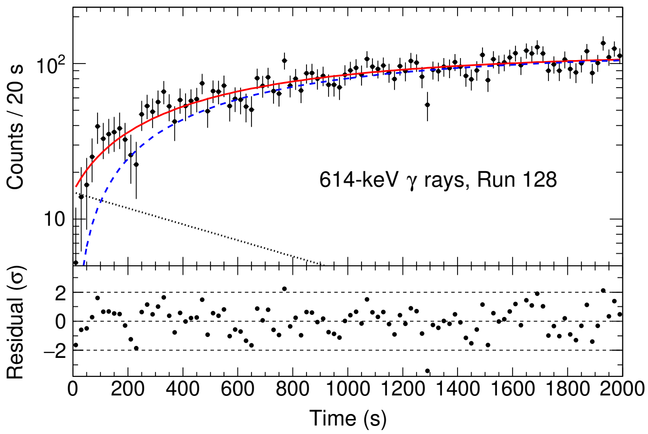

FIG. 11. Background-subtracted time distribution from run 128 for ^{78}Br from the gate on the 614-keV γ ray. The distribution was fitted (solid red line) by an exponential growth function (dashed blue line) plus exponential decay function (dotted black line). The corresponding normalized residuals of the fit are plotted below the time distribution, dashed lines in this plot mark values of -2σ, 0σ, and 2σ.

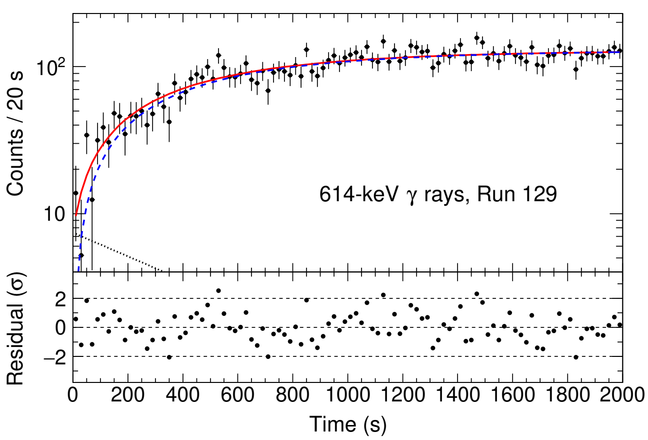

FIG. 12. The same as Fig. 11, but for run 129.

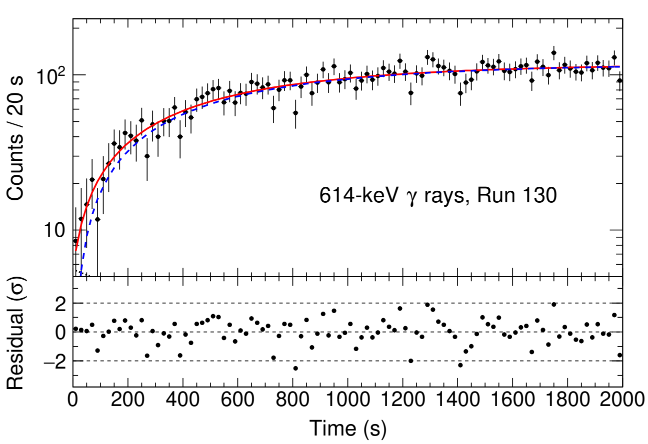

FIG. 13. The same as Fig. 11, but for run 130.

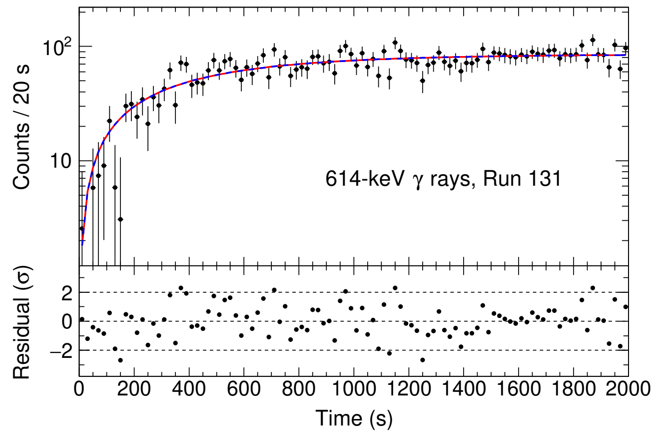

FIG. 14. The same as Fig. 11, but for run 131.

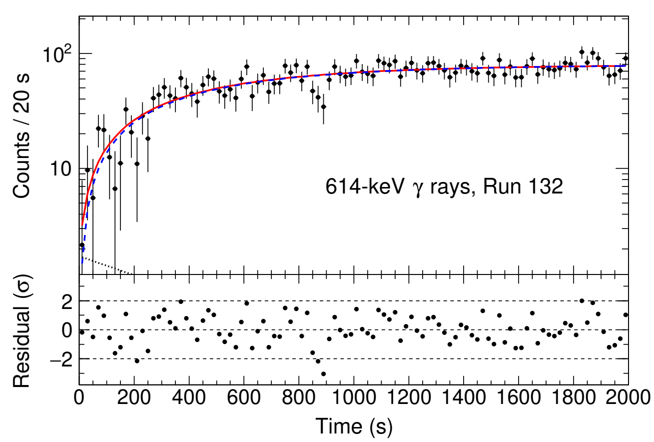

FIG. 15. The same as Fig. 11, but for run 132.

[1] K. Auranen and E. A. McCutchan, Nucl. Data Sheets **168**, 117 (2020).
[2] S. Zhu and E. A. McCutchan, Nucl. Data Sheets **175**, 1 (2021).
[3] A. R. Farhan and B. Singh, Nucl. Data Sheets **110**, 1917 (2009).
[4] Yu. Khazov, A. A. Rodionov, S. Sakharov, and B. Singh, Nucl. Data Sheets **104**, 497 (2005).
[5] A. A. Sonzogni, Nucl. Data Sheets **103**, 1 (2004).
[6] D. Abriola, M. Bostan, S. Erturk, M. Fadil, M. Galan, S. Juutinen, T. Kibédi, F. Kondev, A. Luca, A. Negret, *et al.*, Nucl. Data Sheets **110**, 2815 (2009).
[7] Jun Chen, Nucl. Data Sheets **146**, 1 (2017).
[8] Jun Chen, Nucl. Data Sheets **140**, 1 (2017).
[9] M. J. Martin, Nucl. Data Sheets **108**, 1583 (2007).
[10] A. Negret and B. Singh, Nucl. Data Sheets **124**, 1 (2015).
[11] T. Kibédi, T. W. Burrows, M. B. Trzhaskovskaya, P. M. Davidson, and C. W. Nestor Jr., Nucl. Instrum. Methods A **589**, 202 (2008), `http://bricc.anu.edu.au/`.
[12] A. I. Morales, G. Benzoni, A. Gottardo, J. J. Valiente-Dobón, N. Blasi, A. Bracco, F. Camera, F. C. L. Crespi, A. Corsi, S. Leoni, *et al.*, Phys. Rev. C **89**, 014324 (2014).
[13] J. Kurpeta, A. Andreyev, J. Äystö, A.-H. Evensen, M. Huhta, M. Huyse, A. Jokinen, M. Karny, E. Kugler, J. Lettry, *et al.*, Eur. Phys. J. A **7**, 49 (2000).
[14] F. G. Kondev, M. Wang, W. J. Huang, S. Naimi, and G. Audi, Chin. Phys. C **45**, 030001 (2021).